A signaling axis involving CNOT3, Aurora B and ERK promotes mesendodermal differentiation of ES cells in response to FGF2 and BMP4

Moumita Sarkar[1,4], Matteo Martufi[1,4], Monica Roman-Trufero[1,4], Yi-Fang Wang[2], Chad Whilding[3], Dirk Dormann[3], Pierangela Sabbattini[1], Niall Dillon[1*].

[1] Gene Regulation and Chromatin Group, [2] Bioinformatics and Computing, [3]Microscopy Facility, MRC London Institute of Medical Sciences, Hammersmith Hospital Campus, Du Cane Road, London W12 0NN, UK.

[4]These authors contributed equally to the study

*Correspondence to niall.dillon@lms.mrc.ac.uk

ABSTRACT

Mesendodermal cells are key intermediate progenitors that form at the early primitive streak (PrS) and give rise to mesoderm and endoderm in the gastrulating embryo. We have identified an interaction between CNOT3 and the cell cycle kinase Aurora B that regulates MAPK/ERK signalling during mesendodermal differentiation. Aurora B phosphorylates CNOT3 at two sites that are located close to a nuclear localization signal and promotes nuclear localisation of CNOT3 in mouse ES cells (ESCs) and metastatic lung cancer cells. Mutation of these sites in ESCs gives reduced numbers of embryoid bodies that are largely composed of ectoderm and interferes with differentiation of ESCs into mesendoderm in response to FGF2, BMP4, Wnt3 and Activin. The double mutation affects interaction of CNOT3 with Aurora B and ERK and reduces phosphorylation of ERK in response to FGF2. Our results identify a signalling axis involving CNOT3 that regulates a key pathway in embryogenesis and cancer.

INTRODUCTION

Gastrulation in mammals and birds is initiated by differentiation of mesendodermal (ME) cells, which form at the primitive streak (PrS) as transient precursors expressing both mesodermal and endodermal markers in response to signalling from the visceral endoderm (VE)[1,2]. Ingression of ME cells along the midline of the PrS during gastrulation is accompanied by differentiation into mesoderm and definitive endoderm and formation of the embryonic germ layers.

Signalling ligands that have been shown to be involved in specifying ME differentiation and PrS formation in the early embryo include Wnt3 Activin, BMP4 and FGF2[3-7]. In combination, these ligands can be used to induce ESC differentiation into ME, which is characterised by expression of the mesodermal marker Brachury and endodermal markers GATA4, GATA6 and FOXA2 (reviewed in [8]). The FGF/MEK/ERK signaling pathway plays a vital role in the formation of ME in mouse and human ESCs[2, 9]. The known involvement of the ERK/MAPK pathway in regulating an extremely diverse range of cellular processes at all stages of development[10], implies the existence of multiple secondary levels of regulation that direct ERK/MAPK signals towards their different targets. Adaptor proteins that bind more than one signalling component are one type of mechanism that can be used to regulate ERK/MAPK activity and channel it towards specific targets in a given cell type[11, 12].

CNOT3 was first identified as a component of the CCR4-Not complex, which is involved in regulating transcription and RNA processing in the nucleus and mRNA turnover in the cytoplasm[13]. Studies in ES cells have shown that CNOT3 acts in conjunction with the transcription factors cMYC and ZFX to form part of a transcriptional regulatory module, that binds to a number of gene

promoters in ESCs[14] and has been reported to inhibit differentiation of ESCs into extraembryonic lineages[14, 15]. Knockout of *Cnot3* in the mouse leads to embryonic lethality at the blastocyst stage caused by loss of inner cell mass cells[16]. In addition to its early embryonic functions, CNOT3 has been shown to have important roles in B lymphopoesis[17] and maintenance of adipose tissues[18] in adult mice. *Cnot3* has also been shown to have tumour suppressor and tumour promoting properties[19-21]. Mutations that alter the protein sequence have been identified in a range of cancers, with the largest number observed in prostate and colon cancers[22, 23]. The diverse biological and cellular roles of CNOT3 and the presence of a specialist protein-protein interaction domain, the NOT box, near the C-terminal of the protein suggest that it could function as an adaptor that mediates cross-talk between different cellular pathways.

Here we show that CNOT3 acts as an adaptor that links the cell cycle kinase Aurora B with the MAPK/ERK signalling pathway. Phosphorylation of CNOT3 by Aurora B at sites adjacent to a nuclear localisation signal (NLS) promotes localisation of CNOT3 to the nucleus and increases interaction between ERK and CNOT3. Mutation of the Aurora B target sites in ESCs reduces the level of active phosphorylated ERK in the nucleus, preventing efficient differentiation of ME in response to FGF. We also present evidence that Aurora B-mediated phosphorylation and nuclear localisation of CNOT3 plays an important role in the tumour promoting effects of CNOT3.

RESULTS

Phosphorylation by Aurora B localises CNOT3 to ESC nuclei. The Aurora B cell cycle kinase phosphorylates multiple protein targets during mitosis and

cytokinesis (reviewed in [24]) and is also involved in regulating the G1 to S-phase transition[25, 26]. Upregulation of Aurora B protein levels has been shown to be a marker for lymph node metastasis in lung, colon and breast cancers[27-29]. We initially identified CNOT3 as a potential Aurora B target in a co-immunoprecipitation screen for proteins that bind to Aurora B in primary activated mouse B lymphocytes[30], (A. Frangini, M. Martufi and N. Dillon, unpublished data). Because of the known role of CNOT3 in pluripotency and lineage choice in ES cells, we tested whether it interacts with Aurora B in ESCs. Co-immunoprecipitation of ES cell extracts with anti-Aurora B antibody showed a strong interaction between CNOT3 and Aurora B in ESCs (Figure 1a). Direct interaction of CNOT3 with Aurora B was demonstrated by in vitro pulldown of CNOT3 with GST-tagged Aurora B (Figure 1b).

In vitro phosphorylation by Aurora B in the presence of ^{32}P-ATP showed labelling of a CNOT3 fragment containing amino acids 275-480, indicating the presence of target sites for Aurora B phosphorylation in this region (Figure 1c). Mass spectrometry analysis of in vitro phosphorylated CNOT3 showed that in vitro phosphorylation occurs at residues T292 and S294 in the CNOT3 protein (Supplementary Figure 1a). Examination of the sequence revealed that the T292 is part of a consensus Aurora B phosphorylation site (^{290}R-S-T^{292}) located adjacent to a sequence motif (^{286}K-K-R-G-R^{290}) (Figure 1d), which has been shown to form part of a functional nuclear localisation sequences (NLS) in the *Toxoplasma gondii* GCN5-B histone acetyl transferase and the Influenza D virus nucleoprotein[31-33]. This led us to consider the possibility that phosphorylation by Aurora B might affect the nuclear localisation of CNOT3. To address this question, we first transfected V5-tagged CNOT3 expression constructs carrying

mutations of either T292 or S294, or of both residues, to alanine, into HEK293 cells. The results showed reduction of nuclear CNOT3 for each of the single mutants and the double mutation, indicating that both sites contribute to nuclear localisation in this assay (Figure 1e).

In order to directly test the role of the two residues in regulating nuclear localization of endogenous CNOT3, the T292 and S294 residues were simultaneously mutated to alanine in mouse ESCs using CRISPR/Cas9 (Figures 1d and S1b). Generation of three ESC clones that were homozygous for the T292A/S294A double mutation was confirmed by sequencing (Supplementary Figure 1b). The mutant ESCs grew normally and had the characteristic high S-phase cell cycle profile of ESCs, although there was a small reduction in the proportion of S-phase cells compared with wild-type ESCs (Supplementary Figure 1d and 1e). Analysis of CNOT3 localisation by western blotting of nuclear and cytoplasmic fractions from mutant and wild-type (WT) ESCs showed a reduction in the amount of CNOT3 in the nuclei of mutant ESCs compared with WT cells (Figure 1f). Cytoplasmic levels of CNOT3 were largely unchanged in the mutant cells. These results provide strong evidence that phosphorylation of T292/S294 is involved in specifying localisation of CNOT3 to the ESC nucleus.

To determine whether the effect on nuclear localisation of CNOT3 is mediated by Aurora B, wild-type ESCs were incubated for 24 and 48 hours with the specific Aurora B inhibitor AZD1152. Comparison of the levels of CNOT3 in the nuclear and cytoplasmic fractions after 24 hours incubation with AZD1152 showed a substantial reduction in the amount of CNOT3 in the nucleus (Figure 1g) and the level was further reduced after 48 hours of treatment. The level of CNOT3 in the cytoplasm was largely unaffected (Figure 1g). Propidium iodide

staining and FACS analysis of the sorted cells showed only a minimal effect on the cell cycle with small increases observed in the numbers of G1 and G2 cells at both time points and and a small reduction in the number of S-phase cells at the 48 hour time point (Supplementary Figure 1c and 1e).

Effect of mutating CNOT3-T292/S294 on embryoid body formation. We set out to test whether the absence of phosphorylation of CNOT3-T292/S294 affected pluripotency and differentiation potential of the mutated ESCs. Wild-type and mutant ESCs were cultured under conditions that promoted the formation of embryoid bodies (EBs) (see Methods for details). EB formation was assessed after 4, 8 and 10 days of incubation under these conditions. The results show that the double *Cnot3* mutation (*Cnot3*-DM) resulted in a 40% reduction in EB numbers after 10 days in culture and the average size of the EBs was reduced by 40-50% (Figure 2a and b).

Staining of the EBs for the lineage markers Brachyury (mesoderm), FOXA2 (Endoderm) and Nestin (Ectoderm) revealed a striking difference between the wild-type and *Cnot3*-DM EBs (Figure 2c). The EBs formed from wild-type ESCs showed strong staining for all three markers, with Brachyury giving broad staining of the central and peripheral regions of the EBs, whereas FOXA2 staining was more restricted to the central regions. The ectodermal Nestin staining was localised to the periphery of the EBs. In contrast, the *Cnot3*-DM EBs showed very low staining for Brachyury or FOXA2 and strong staining for Nestin that was located both centrally and at the periphery of the EBs (Figure 2c). The pattern of ectodermal staining in the mutant EBs was confirmed by staining for the ectodermal marker OTX2 (Supplementary Figure 2a). These

results show that the mutant EBs were predominantly composed of ectoderm, which suggests that blocking phosphorylation of CNOT3-T292/S294 interferes with germ layer formation.

CNOT3-T292/S294 phosphorylation promotes ME differentiation.

Formation of mesoderm and endoderm during gastrulation is thought to involve transtioning of cells through an intermediate ME stage at the PrS [34-36]. Nodal/Activin, Bmp, Wnt and FGF signaling pathways have been shown to have critical roles in ME differentiation [2, 3, 9, 37-39]. To investigate the role of CNOT3-T292/S294 phosphorylation in ME formation, we carried out differentiations in a defined medium containing BMP4 and FGF2 and different combinations of Activin, Wnt and the GSK3β inhibitor CHIR99021, which stabilises β-catenin, bypassing Wnt activation[40] (Figure 3a-c) (see Methods).

When applied to wild-type cells, all of the combinations that included BMP4 and FGF2 and either Wnt, Activin or CHIR99021 gave a high proportion of ME cells that stained for Brachyury and FOXA2 (Figure 3c). Incubation with FGF2 and BMP4 alone also promoted ME differentiation, but the numbers of differentiated cells was lower. Analysis of the mutant cells showed that differentiation in the presence of all ligand combinations tested gave significantly reduced numbers of differentiated cells (Figure 3b). The largest reductions in the number of mutant cells relative to wild-type were obtained with Wnt + FGF2 + BMP4 (80%) and FGF2 + BMP4 (65%). This result points to a cooperative stimulating effect of Wnt3, BMP4 and FGF2 on ME differentiation that is dependent on CNOT3 phosphorylation by Aurora B. The results also

provide an explanation for the very strong effect that the T292A/S294A double mutation has on differentiation of mesoderm and endoderm in embryoid bodies.

The ability of the wild-type and *Cnot*3-DM cells to differentiate directly into mesoderm, endoderm and ectoderm was also tested (Supplementary Figure 2b) (see Methods). Only in the case of differentiation into endoderm induced by FGF2 and retinoic acid, did we observe reduced differentiation of the mutant cells compared with the levels observed for wild-type cells (Supplementary Figure 2b). These findings support the idea that the regulatory role of CNOT3-T292/S294 phosphorylation is linked to specific signalling pathways and suggest that FGF signalling is one of these pathways.

Survival of ME cells is enhanced by CNOT3 phosphorylation. A more detailed characterisation of the effect of the *Cnot3*-T292A/S294A mutation on FGF2 and BMP4 signalling from day 2 to day 8 of ME differentiation showed reduced numbers of *Cnot3*-DM cells from day 2 onwards (Figure 4a, b). Staining for additional mesodermal and endodermal lineage markers (SMA: mesoderm; GATA4: endoderm) confirmed ME differentiation (Figure 4c-e) The conclusion that proliferation and survival of ME cells is strongly affected by the double mutation was further reinforced by the results of a time-lapse analysis of the differentiating wild-type and mutant cells between 4 and 8 days of ME differentiation (Supplementary Video 1). The time-lapse analysis showed an explosive proliferation of the wild-type cells, whereas the *Cnot3*-DM cells failed to expand and appeared to undergo high rates of cell death following cell division. Analysis of the differentiation capacity of the other two *Cnot3*-T292A/S294A mutant clones that were generated by the CRISPR/CAS9 targeting

showed a similar failure to expand and proliferate in the mesendoderm differentiation medium (Supplementary Figure 3a), confirming that the effect was caused by the double mutation. The cell cycle profiles of the wild-type and mutant cells after 4 days of differentiation were similar, implying that the major effect of the mutation was on survival of differentiating mesendoderm cells (Supplementary Figure 3b).

The susceptibility of the *Cnot3*-DM cells to apoptosis during ME differentiation in response to FGF2 and BMP4 was directly assessed by staining wild-type and mutant cells with Annexin V and also by measuring propidium iodide (PI) uptake after 4 days of differentiation. The wild-type cells showed almost no staining for either apoptotic marker whereas the 4-day differentiated mutant cells were strongly stained for PI and Annexin V, indicating that the failure of the mutant cells to differentiate was associated with high rates of apoptosis (Figure 4f). This result suggests a functional relationship between CNOT3 phosphorylation and survival signals mediated by incubation with FGF2 and BMP4.

Gene expression analysis by RT-qPCR was also used to examine differences in mRNA levels for lineage and cell survival markers between the wild-type and mutant ME differentiated in response to FGF2/BMP4. The results showed upregulation of mesodermal (*Brachury* and *MixL1*) and endodermal (*Gata4*, *Gata6*, *Sox17*, *Pdgfr*, *Cxcr4*) genes during differentiation of wild-type cells, confirming differentiation into ME (Figure 5a). Genes that are involved in mesenchymal, placental and epithelial cell development and *Cdx2*, which is expressed in endoderm and trophectoderm, were upregulated. However, expression of the early trophectoderm marker *Tead4* was very low (Figure 5a),

indicating that the *Cnot3*-DM cells did not show a propensity to differentiate into trophectoderm under these conditions.The mRNA and protein levels of ME genes were not significantly altered in the *Cnot*-DM cells compared with wild-type cells, with the exception of *Brachury* (Figure 5b and 5c). These conclusions were reinforced by a transcriptomic comparison of the wild-type and *Cnot3*-DM cells using RNA-seq (Supplementary Figure 4a and 4b). The RNA-seq analysis showed that 153 genes were significantly upregulated and 155 were downregulated in the mutant cells (Supplementary Tables 2a and 2b). Gene Ontology and GSEA analysis revealed that the mutation resulted in increased expression of genes that are associated with cell death and apoptosis (Supplementary 4c and 4e). In addition, genes involved in cell proliferation were downregulated (Supplementary Figure 4d). The RNA-seq analysis also showed that the level of mRNA for FGFR1 which is the major FGFR that promotes ME differentiation[41-43] was unchanged in the *Cnot3*-DM cells, whereas reduced expression was observed for FGFR2, which has a major role in trophectoderm differentiation[44].

Mutating CNOT3-T292/S294 reduces ERK phosphorylation. ERK1/2 signalling in response to stimulation by FGF is one of the major events that directs the transition from the pluripotent state to lineage commitment to the three germ layers and is critical for gastrulation [45, 46]. FGFs acts through the FGF receptors (FGFRs) to activate the Ras/MEK ERK pathway, which culminates in phosphorylation of MAPK/ERK at the threonine and tyrosine residues of the TEY motif [10]. Phospho-ERK is imported into the nucleus where it phosphorylates a number of transcription factors that are associated with proliferation as well as phosphorylating members of the RSK and MSK kinase families (reviewed in [10]).

There is also cross-talk between Wnt signalling and the Ras/MEK/ERK pathway, with Wnt signalling upregulating ERK phosphorylation by inhibiting GSK3β and preventing it from phosphorylating and destabilising Ras [47, 48]. ERK has been reported to upregulate Aurora B expression in melanoma cells [49] and phosphorylated ERK plays important roles in cell survival [50].

Involvement of the FGF/MEK/ERK pathway in signalling cell survival during ME differentiation was supported by the observation that treatment of the cells with FGF and MEK inhibitors caused a dramatic reduction in cell numbers (Figure 6a). This led us to consider the possibility of a functional interaction between Aurora B, CNOT3 and ERK that would cause the CNOT3 double mutation to affect ERK phosphorylation and cell survival. To assess the effect of the *Cnot3*-DM mutation on ERK phosphorylation, extracts from wild-type and mutant ESCs that had been differentiated with FGF2 and BMP4 for 4 days were analysed by western blotting using an antibody that recognised the phosphorylated ERK TEY motif [10] and an antibody against total ERK. The results showed a strong reduction in the level of phosphorylated ERK in the *Cnot3*-DM cells compared to wild-type (Figure 6b). Levels of phosphorylated ERK and ERK1/2 were unaffected in undifferentiated *Cnot3*-DM ESCs (Supplementary Figure 5a). A similar reduction of phosphorylated ERK was observed when the differentiated cells were treated with AZD1152, further confirming the role of Aurora B-mediated phosphorylation of CNOT3 in activating ERK (Figure 6c). Aurora B and CNOT3 continue to interact in differentiating ME cells, as shown by immunoprecipitations carried out with anti-CNOT3 antibody on extracts from the 4 day differentiated cells (Figure 6d). Levels of CNOT3 were reduced in differentiated *Cnot3*-DM cells (Figure 5B), suggesting that phosphorylation by

Aurora B stabilises wild-type CNOT3, similar to the effect that has been reported for Aurora B and Aurora C phosphorylation of INCENP[51].

Altered interaction of mutant CNOT3 with Aurora B and ERK. To analyse interactions between CNOT3, Aurora B and ERK at the single-cell level during ME differentiation, we made use of the proximity ligation assay (PLA). ESCs were incubated for 4 days in differentiation medium containing FGF2 and BMP4 and then subjected to PLA using mouse anti-Aurora B and rabbit anti-CNOT3 antibodies. (see Methods). The results of this analysis showed a high level of association between CNOT3 and Aurora B in wild-type cells after 4 days of differentiation (Figures 7a and S6b). The number of interaction foci in the nuclei of wild-type cells was around half the number observed in the cytoplasm.

Analysis of the *Cnot3* mutant cells showed an unexpected increase of approximately 3-fold in the interaction between CNOT3 and Aurora B in the mutant cells compared to the wild-type cells after 4 days of ME differentiation (Figure 7a). The increased signal was accompanied by an increase in the proportion of interaction foci observed in the nucleus compared to wild type cells. Overall, these results confirm the strong interaction between CNOT3 and Aurora B that was observed by co-IP of extracts from undifferentiated ESCs and after 4 days of ME differentiation. The differences between the interaction patterns observed in the wild-type and Cnot3-T292A/S294A mutant cells suggest that phosphorylation of T292/S294 by Aurora B plays an important role in regulating the dynamic behaviour of CNOT3 in differentiating ME cells.

PLA of the interaction between CNOT3 and ERK showed a substantial level of interaction in wild-type 4-day differentiated cells that was broadly

distributed between cytoplasmic and nuclear compartments. The mutant cells showed significant reductions in both compartments, with the cytoplasm showing a 3-fold reduction and the nuclei a 5-fold reduction in the number of interaction foci observed (Figure 7b). These results, which were confirmed with a second, separate anti-CNOT3/anti-ERK antibody pair (Supplementary Figure 6a), provide strong evidence that ERK interacts with CNOT3 and that this interaction is promoted by Aurora B-mediated phosphorylation of CNOT3-T292/S294. The observation that mutation of the Aurora B phosphorylation sites reduces phosphorylation of ERK suggests that the interaction between ERK and phosphorylated CNOT3 promotes or stabilises ERK phosphorylation, thereby enhancing Ras/MEK/ERK signalling.

Phosphorylation alters localisation of CNOT3 in cancer cells. Mutations in the coding region of human *Cnot3* have been observed in a number of cancers[22], with genetic analysis providing evidence that *Cnot3* mutations can have tumour suppressor[19] and tumour promoting[52] effects. High levels of nuclear CNOT3 have also been observed in an aggressive colorectal cancer cell line[21]. These observations, together with our results, led us to consider the possibility that Aurora B might be promoting nuclear localisation and EMT in cancer cells. To test this hypothesis, H1299 and A549 non-small cell lung cancer (NSCLC) cells were stained with anti-CNOT3 antibody. H1299 was originally derived from a lymph node metastasis and A549 from a lung adenocarcinoma. The results of the immunofluorescence analysis (Figure 8a) showed that nuclear CNOT3 levels were approximately 2-fold higher than the cytoplasmic levels in H1299 cells,

whereas the localisation of the protein was evenly distributed between nucleus and cytoplasm in A549 cells.

Involvement of Aurora B phosphorylation in the H1299-specific localisation of CNOT3 was investigated by treating H1299 cells for 3 hours with AZD1152. The incubation time was optimised to avoid disruption of the cell cycle. The results show a dramatic effect of Aurora B inhibition on CNOT3 localisation in the H1299 cells with the nuclear levels of CNOT3 in the inhibitor-treated cells reduced by 3-fold relative to the cytoplasmic level (Figure 8b).

The involvement of the NLS and the Aurora B target sites in cancer is further supported by the recent identification of a *Cnot3*-K286E mutation in 11% (4/37) of a cohort of pre-malignant adenomas from that were sequenced from Familial Adenomatous Polyposis patients[52] (Figure 8c). *Cnot3*-K286 is the first residue of the KKRGR nuclear localisation sequence that operates in conjunction with Aurora B phosphorylation to promote nuclear uptake of Aurora B in mouse ESCs. Mutations that affect the first residue of the Aurora B consensus (*Cnot3*-R290C and -R290H) have also been described in one lung and three colorectal cancers[22, 53, 23]. Overall, a total of nine cancer patients have been shown to have mutations in the NLS (Figure 8c). This clustering of mutations provides strong evidence of a role for this region in oncogenic progression, particularly in colorectal cancers. The R286E, R290H and R290C mutations would be expected to reduce nuclear uptake of CNOT3 in response to Aurora B, leading to downregulation of ERK phosphorylation. This is consistent with reports that ERK, in addition to its tumour promoting properties, can also act as a tumour suppressor by potentiating oncogene-induced sensescence[54].

DISCUSSION

We have identified a role for the CNOT3 protein in regulating the signalling pathways that promote ME differentiation, a process that is critical for gastrulation in the mammalian embryo. The effect occurs through interaction between CNOT3 and Aurora B, with phosphorylation of CNOT3 by Aurora B increasing its localization to the nucleus and promoting interaction with MAPK/ERK proteins and upregulation of ERK activity. Interference with phosphorylation by mutation of the Aurora B target sites in ESCs led to a dramatic reduction in differentiation of mesoderm and endoderm during embryoid body formation, with the mutant EBs being largely made up of ectoderm.

FGF2/ERK signalling plays vital roles in specification of mesoderm and endoderm as well as being a key factor for cell survival [8, 9, 55-57]. Analysis of ERK phosphorylation showed that ERK phosphorylation and activation is strongly reduced by the *Cnot3* double mutation. This finding provides a direct mechanistic explanation for the increased apoptosis and inefficient differentiation observed in the *Cnot3*-DM cells when differentiation is induced using FGF2 and ERK. Phosphorylation of ERK by MEK is followed by rapid import of phospho-ERK into the nucleus, which occurs through a variety of mechanisms [50]. The level of phospho-ERK in the nuclear compartment is known to be strongly dependent on binding of ERK to stabilising proteins in the cytoplasm and in the nucleus [50, 58, 59] Our results indicate that ERK interacts with CNOT3 in differentiating ME cells and that this interaction is reduced in the *Cnot3*-DM cells by 3-fold in the cytoplasm and by 5-fold in the nucleus. Together with the observation that Aurora B phosphorylation promotes localization of

CNOT3 to the nucleus, this suggests that the interaction between phosphorylated CNOT3 and ERK could be involved in stabilising phospho-ERK in the cytoplasmic and nuclear compartments and potentially in the transport of phospho-ERK into the nucleus. CNOT3 has been shown to interact with transcription factors[14, 17], raising the possibility that it could act as a vehicle for recruitment of activated phospho-ERK to gene promoters, which are the target for many of the effector functions of ERK.

The large increase in the level of interaction between CNOT3 and Aurora B that was observed in the *Cnot3*-DM cells suggests that the interaction between Aurora B and wild-type CNOT3 is dynamic, with phosphorylation of CNOT3 leading to rapid release of the kinase from the interaction. Mutation of the phosphorylation sites would block this release by preventing phosphorylation and would lock CNOT3 into the interaction with Aurora B and prevent it from interacting with phospho-ERK (shown schematically in Figure 8d).

Overall, our results provide evidence of a signaling axis between ERK and Aurora B with CNOT3 acting as a key mediator between the two proteins. Our findings suggest that Aurora B acts through CNOT3 to increase the level of phospho-ERK, thereby promoting survival and differentiation of ME cells. These observations indicate that the synergy between the three proteins plays an important role in regulating EMT during ME differentiation and gastrulation of the mouse embryo. The very strong reduction in survival and proliferation that we observe when the *Cnot3*-DM cells are induced to differentiate into ME suggests that Aurora B links up with the MAPK/ERK and Wnt pathways via CNOT3 to promote the explosive expansion of cell numbers that occurs in the embryo at the time of implantation and gastrulation. The increased nuclear

localisation of CNOT3 in an NSCLC cell line that was isolated from a lymph node metastasis and the strong dependence of this localisation on Aurora B activity opens up the possibility that nuclear localisation of CNOT3 in response to Aurora B phosphorylation promotes EMT in cancer cells, acting as a driver for metastasis.

AUTHOR CONTRIBUTIONS

MS, MM, MRT and ND participated in the design of the study. MS identified and characterised the effects of the Cnot3 mutations on mesendodermal differentiation and ERK phosphorylation. MM and MRT carried out the CRISPR targeting in ESCs and the initial characterisation of the nuclear localisation of CNOT3. YFW analysed the RNA-seq data. CW and DD provided microscopy expertise and carried out the digital analysis of the PLA data. PS contributed to the ESC analysis. MS and ND wrote the manuscript with contributions from MM and MRT. ND supervised and coordinated the project.

ACKNOWLEDGEMENTS

We thank Nicola Festuccia, Aida di Gregorio and Sheila Xie for advice and helpful discussions, Holger Kramer and Alex Montoya for assistance with mass spectrometry data analysis. We also thank the staff of the LMS Genomics Facility for HT sequencing, and the LMS/NIHR Imperial Biomedical Research Centre Flow Cytometry Facility for support. This research was funded by the Medical Research Council UK.

DECLARATION OF INTERESTS

The authors declare no competing interests.

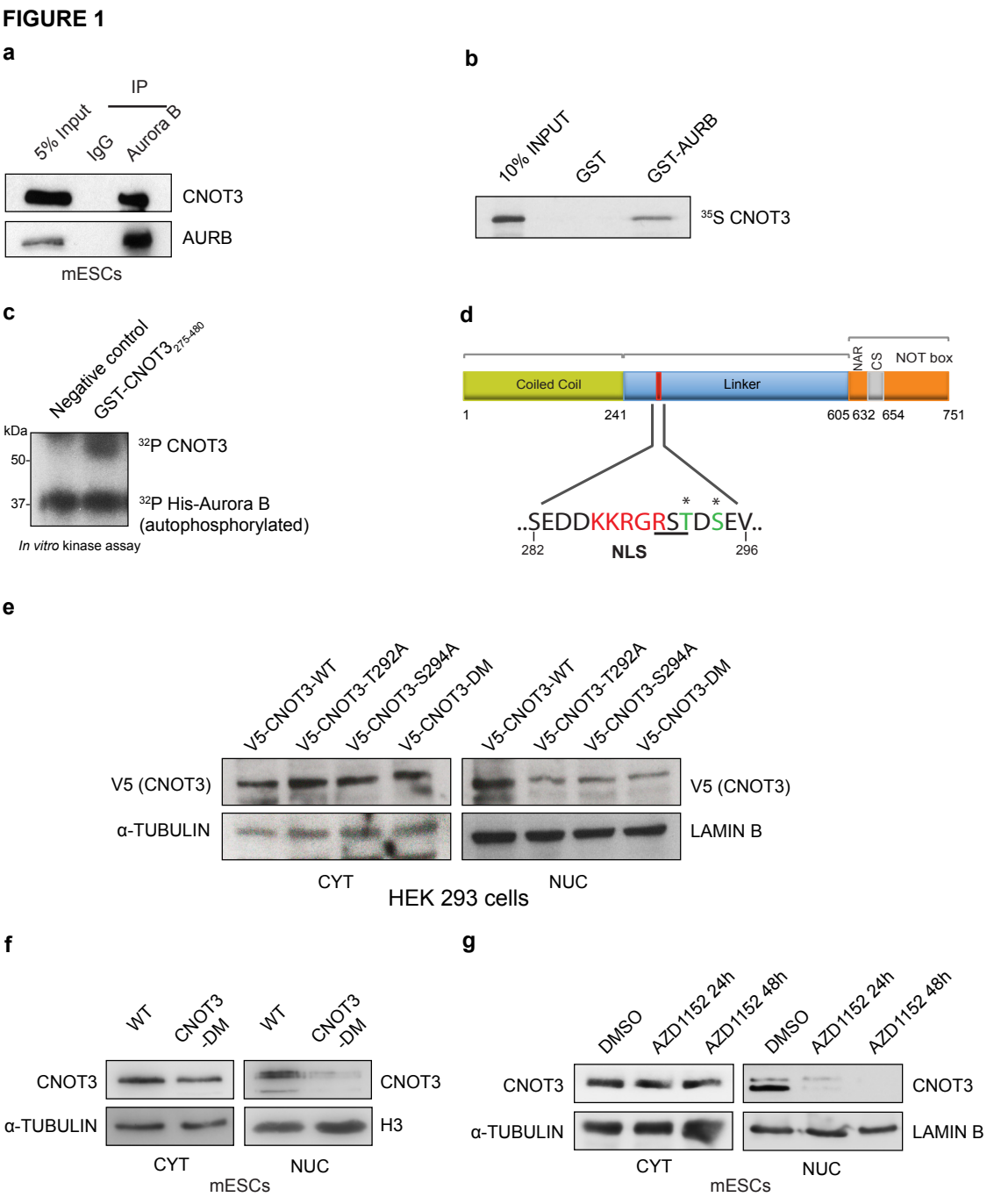

Figure 1: Phosphorylation by Aurora B is increases nuclear localisation of CNOT3. a. Representative immunoprecipitation (IP) carried out on cell extracts prepared from wild-type ESCs using anti-Aurora B antibody. Blots were probed with anti-CNOT3 antibody and anti-Aurora B antibody. IP with normal mouse IgG was used as a negative control. Input = 5% of the extract. **b.** *In vitro* GST

pulldown assay using GST-Aurora B and *in vitro* transcribed/translated CNOT3, labelled with ^{35}SMethionine. GST-only was used as a negative control. Input =10% labelled CNOT3. **c.** *In vitro* kinase assay carried out on the purified GST-CNOT3 275-480 fragment using γ-^{32}P-ATP. The lower band is autophosphorylated Aurora B. Mass spectrometry data (Supplementary Figure 1a) showed that CNOT3-T292 and -S294 are the sites of phosphorylation by Aurora B. The negative control contained all of the reaction components except the GST-CNOT3 fragment. **d.** Schematic representation of the organisation of the domains of CNOT3 [60], showing the position of the consensus nuclear localisation signal (NLS, red type) and the Aurora B consensus phosphorylation site (underlined). **e.** Representative immunoblot analysis of V5 tagged CNOT3 carried out on cytoplasmic and nuclear extracts from HEK 293 cells transfected with single mutant constructs (*Cnot3*-T292A or *Cnot3*-S294A) and the double mutant *Cnot3*-DM. Cells were harvested 48 hours post-transfection. α-Tubulin and Lamin B were used as loading controls for the cytoplasm and nucleus respectively. **f.** Representative immunoblot analysis of CNOT3 levels in cytoplasmic and nuclear extracts of wild-type (WT) and *Cnot3*-DM ESCs. Cytoplasmic loading control: α-Tubulin. Nuclear loading control: Histone H3. **g.** Representative immunoblot analysis of CNOT3 from cytoplasmic and nuclear extracts of WT ESCs, treated with Aurora B inhibitor AZD1152 for 24 hours and 48 hours respectively before harvesting. DMSO: vehicle control. Cytoplasmic loading control: α-Tubulin. Nuclear loading control: Lamin B.

FIGURE 2

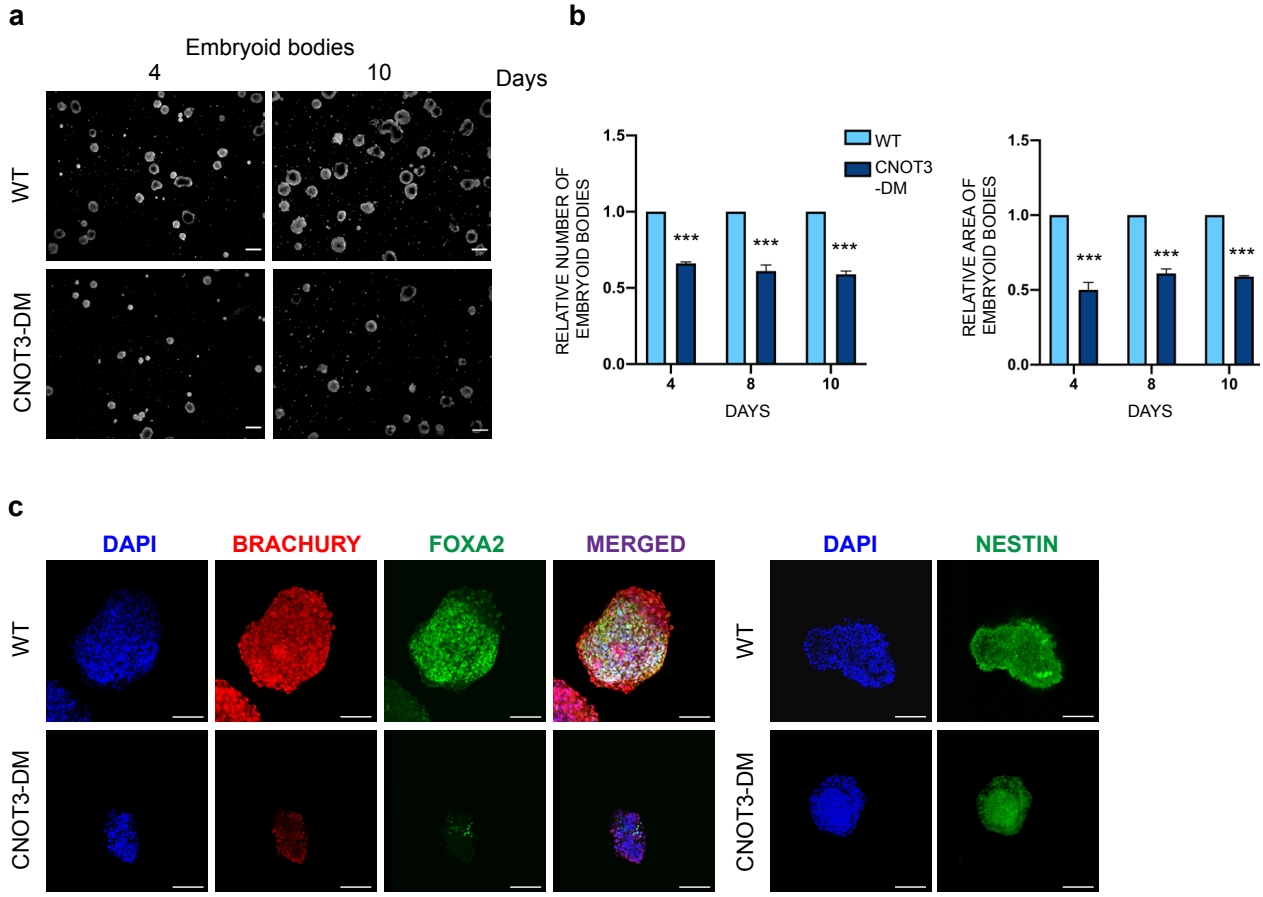

Figure 2: Mutation of CNOT3-T292A/S294 affects EB germ layer formation.

a. Representative phase-contrast images of embryoid bodies (EBs) formed from wild-type (WT) and *Cnot3*-DM ESCs after 4 and 10 days. Scale bar = 100 μm. **b.** Histograms show the number and size (area) of EBs formed from *Cnot3*-DM ESCs relative to WT cells at 4, 8 and 10 days respectively. Mean ± SEM; *t*-test ***P<0.001 *n*=3. **c.** Left panel: Representative confocal images of EBs derived from WT and *Cnot3*-DM ESCs stained with the mesodermal marker Brachury (red) and endodermal marker FOXA2 (green) at 8 days (scale bar = 100 μm). Right panel: staining of WT and mutant EBs for ectodermal marker nestin

(green) (scale bar = 100 μm). Nuclei were stained with DAPI. Staining for an additional ectodermal marker OTX2 is shown in Supplementary Figure 2a.

FIGURE 3

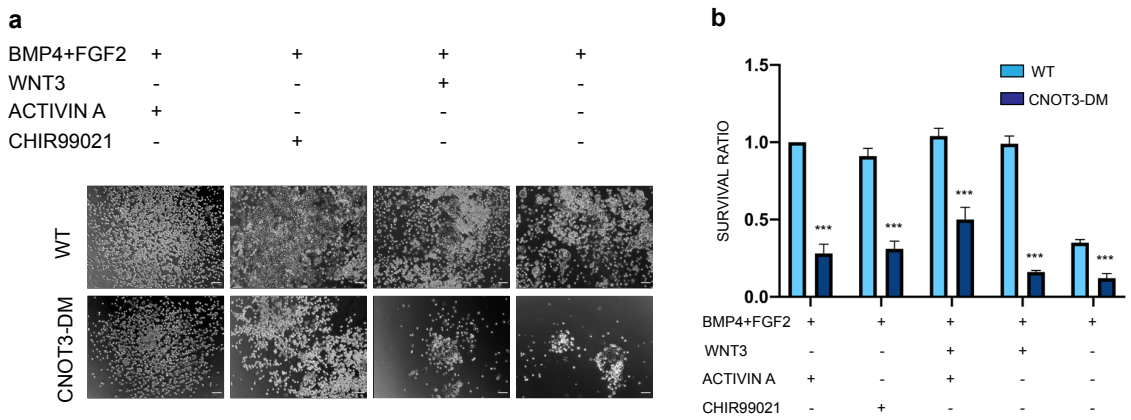

Figure 3: CNOT3 phosphorylation promotes efficient differentiation of ME.

a. Representative phase-contrast images showing the efficiency of mesendoderm (ME) differentiation of WT and *Cnot3*-DM ESCs after 4 days in the presence of various combinations of Activin A, CHIR99021, Wnt3 and BMP4 + FGF2. Scale bar = 100 μm. **b**. Histogram shows the survival of WT and *Cnot3*-DM ESCs treated with different combinations of the ligands used in (**a**) after 4 days of mesendoderm differentiation. Activin A, CHIR99021 and Wnt3 was added after two days of BMP4+FGF2 induced differentiation and the cell survival was determined using WST-1 reagent on day 4 of the differentiation. Survival ratios (mean ± SEM) were calculated relative to the values obtained for WT cells treated with Activin A+ BMP4+FGF2, which was assigned a value of 1. Significance was calculated between WT and CNOT3-DM for each combination using unpaired *t*-test ***P<0.001, *n*=3. **c.** Representative IF images of mesodermal marker Brachury (red) and endodermal marker FOXA2 (green) following BMP4 + FGF2 induced mesendoderm differentiation of WT and *Cnot3*-DM ESCs for 4 days in the presence of combinations of Activin A, CHIR99021 and Wnt3 (as indicated). Merged red and green images show the mesendodermal cells. Nuclei were stained with DAPI; scale bar = 100 μm.

FIGURE 4

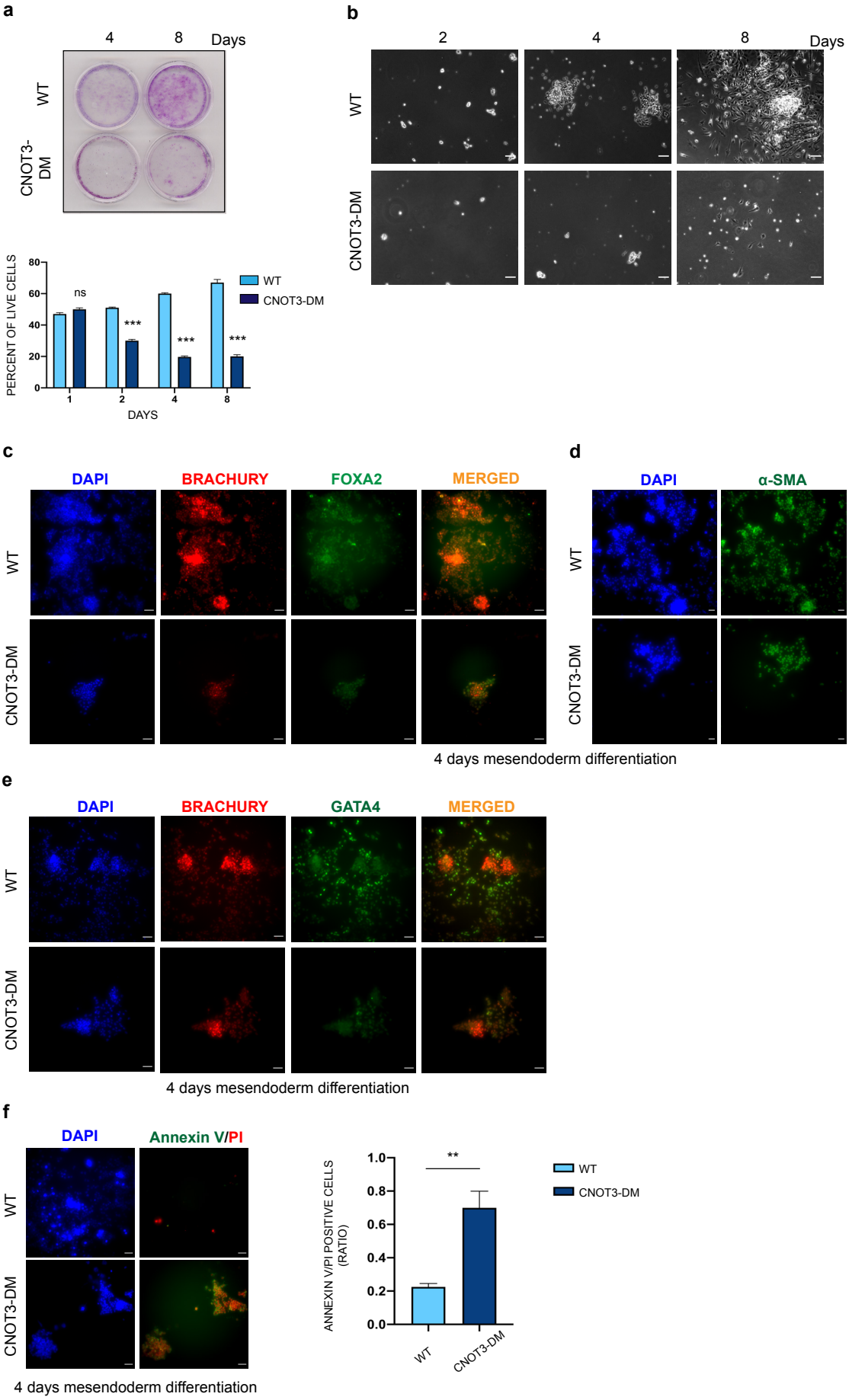

Figure 4: CNOT3 phosphorylation enhances survival of differentiating ME cells. **a**. Top panel: Crystal violet staining showing the efficiency of BMP4 + FGF2 induced mesendoderm differentiation of WT and *Cnot3*-DM ESCs after 4 and 8 days. Bottom panel: At the indicated time-points, live cells were counted based on trypan blue exclusion. Histogram shows the percentage of live cells at different time points of differentiation. Mean ± SEM; unpaired *t*-test between WT and *Cnot3*-DM for each time-point, ***P<0.001 *n*=3. Crystal violet staining of two other independently generated clones of *Cnot3*-T292A/S294A mutant ESCs is shown in Supplementary Figure 3a. **b**. Representative phase-contrast images showing the efficiency of BMP4 + FGF2 induced mesendoderm differentiation of WT and *Cnot3*-DM ESCs for 2, 4, and 8 days. Scale bar: 100 μm. See also Supplementary Video 1 for a time-lapse analysis of the differentiations. **c-e**. Representative IF analyses of images of staining for the mesodermal markers Brachury (red) (**c**) and SMA (green) (**d**) and endodermal markers FOXA2 (green) (**c**) and GATA4 (green) (**e**) carried out on ME cells differentiated from WT and *Cnot3*-DM ESCs by incubating with BMP4 + FGF2 for 4 days. Nuclei were stained with DAPI. Merged red and green images show the ME cells. Scale bars in **c** = 100 μm; scale bar in **d** = 60 μm. For IF analysis at 8 days of differentiation, see Supplementary Figures 3c and Figure 3d. **f**. IF analysis of apoptotic markers Annexin V(green) and PI (red), in cells differentiated for 4 days with BMP4 + FGF2. Merged images show the Annexin V and PI stained apoptotic cells. Nuclei were stained with DAPI; scale bar = 100 μm. Histogram represents ratio of Annexin V/PI positive cells relative to total number of cells. Apoptotic cells were counted from ten randomly chosen fields for each biological replicate. Mean ± SEM; *t*-test **P<0.01 *n*=3.

FIGURE 5

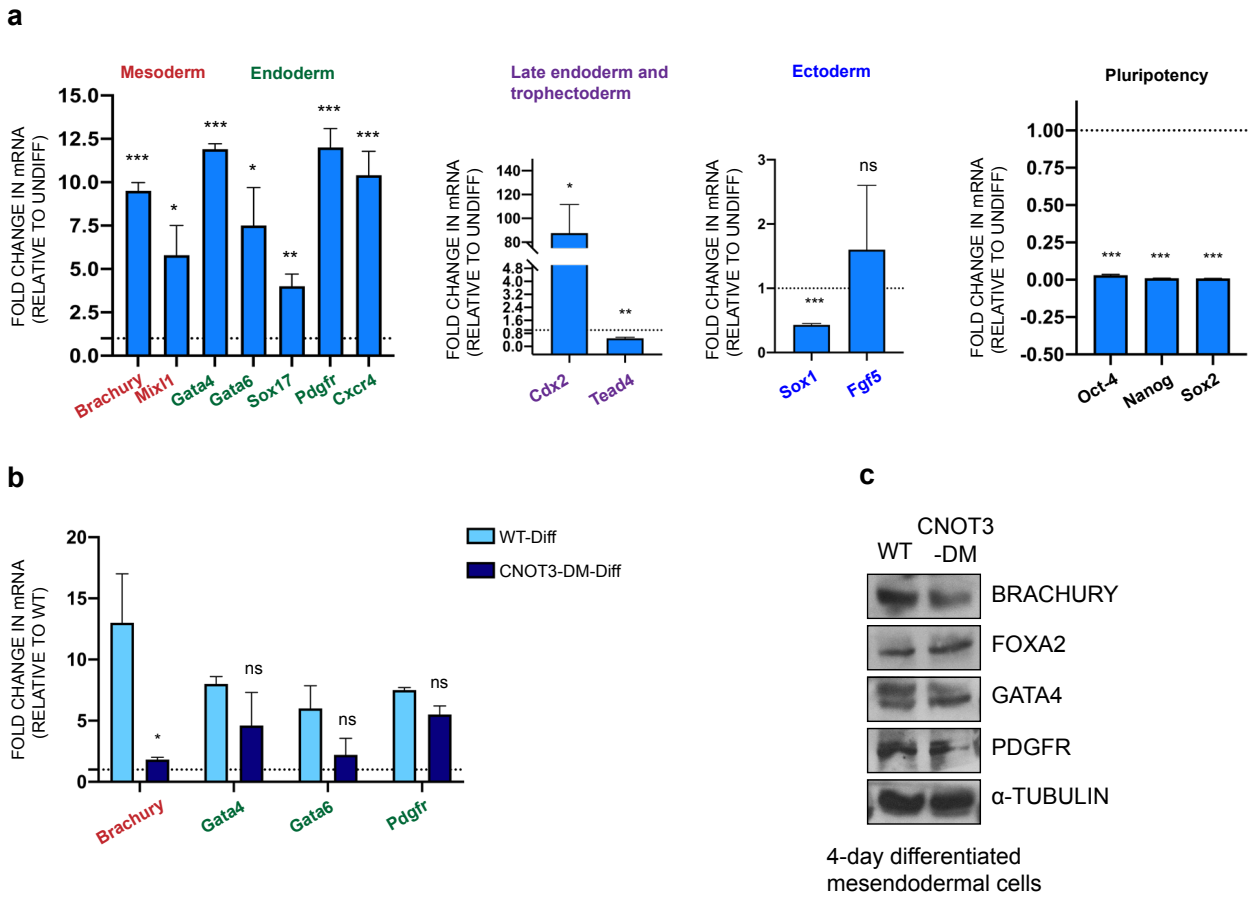

Figure 5: Expression analysis of lineage markers in differentiating *Cnot3*-DM ME cells. **a.** Fold change in mRNA levels of lineage marker genes after BMP4+FGF2 induced differentiation of WT ESCs for 4 days. Values for the undifferentiated (undiff) ESCs were set at 1 as indicated by a horizontal line in each histogram. *Cdx2* is a marker for late endoderm and trophectoderm. *Tead4* is a marker for early trophectoderm. Mean ± SEM; *n*=3. P values calculated by unpaired *t*-test, *P<0.05, ***P<0.001. **b.** Fold change in mRNA levels of ME markers after BMP4+FGF2 induced differentiation of WT ESCs for 4 days. Error bars represent the mean ± SEM; *n*=2. (P values in (**a**) and (**b**) calculated by unpaired *t*-test, *P<0.05, ***P<0.001. **c.** Representative immunoblot analysis of

the indicated lineage markers after BMP4 + FGF2 induced ME differentiation of WT and *Cnot3*-DM ESCs carried out for 4 days. α-Tubulin was used as a loading control.

FIGURE 6

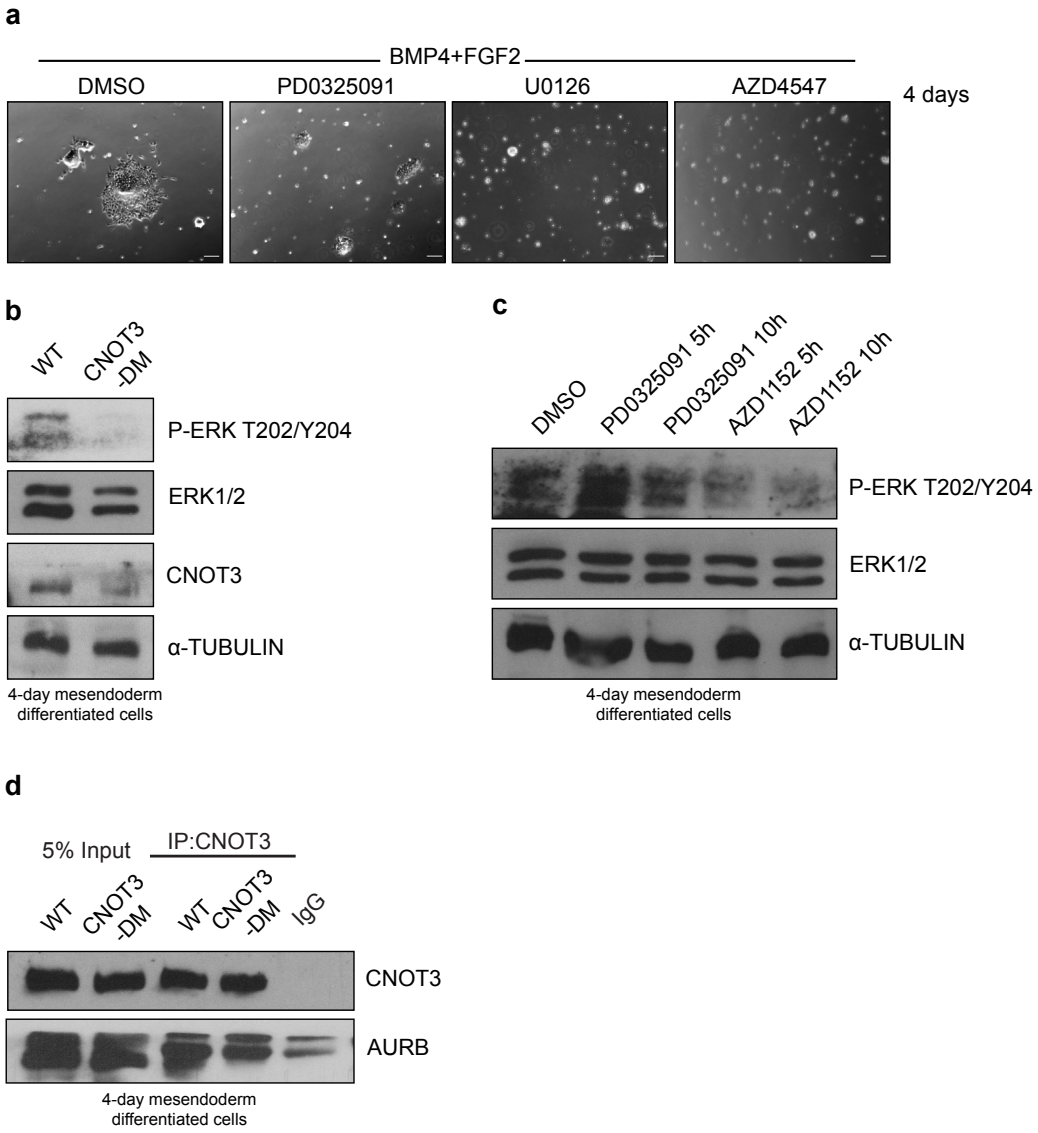

Figure 6: The CNOT3 double mutation reduces ERK phosphorylation during ME differentiation. **a**. Phase-contrast images showing the effects of MEK inhibitors that abolish ERK activity (PD0325091 and U0126), and the FGFR inhibitor AZD4547, on BMP4 + FGF2 induced ME differentiation of WT ESCs carried out for 4 days. Each inhibitor was added after two days of differentiation. Scale bar = 100 μm.

b. Representative immunoblot analysis of the indicated proteins carried out on cell extracts from WT and *Cnot3*-DM ESCs subjected to 4 days of BMP4 + FGF2 induced differentiation into ME. Loading control: α-Tubulin. **c**. Representative immunoblot of WT ESCs differentiated as in **b** and treated with Aurora B inhibitor AZD1152 and MEK inhibitor PD0325091 for 5 hours and 10 hours respectively before harvesting. Loading control: α-Tubulin. **d**. Co-IP was carried out with anti-CNOT3 antibody on cell extracts prepared from WT and *Cnot3*-DM ESCs differentiated as in **b**. Co-immunoprecipitated proteins were immunoblotted and probed with anti-CNOT3 and anti-Auorora B. Negative control: rabbit IgG. Input = 5% of extracts.

FIGURE 7

a

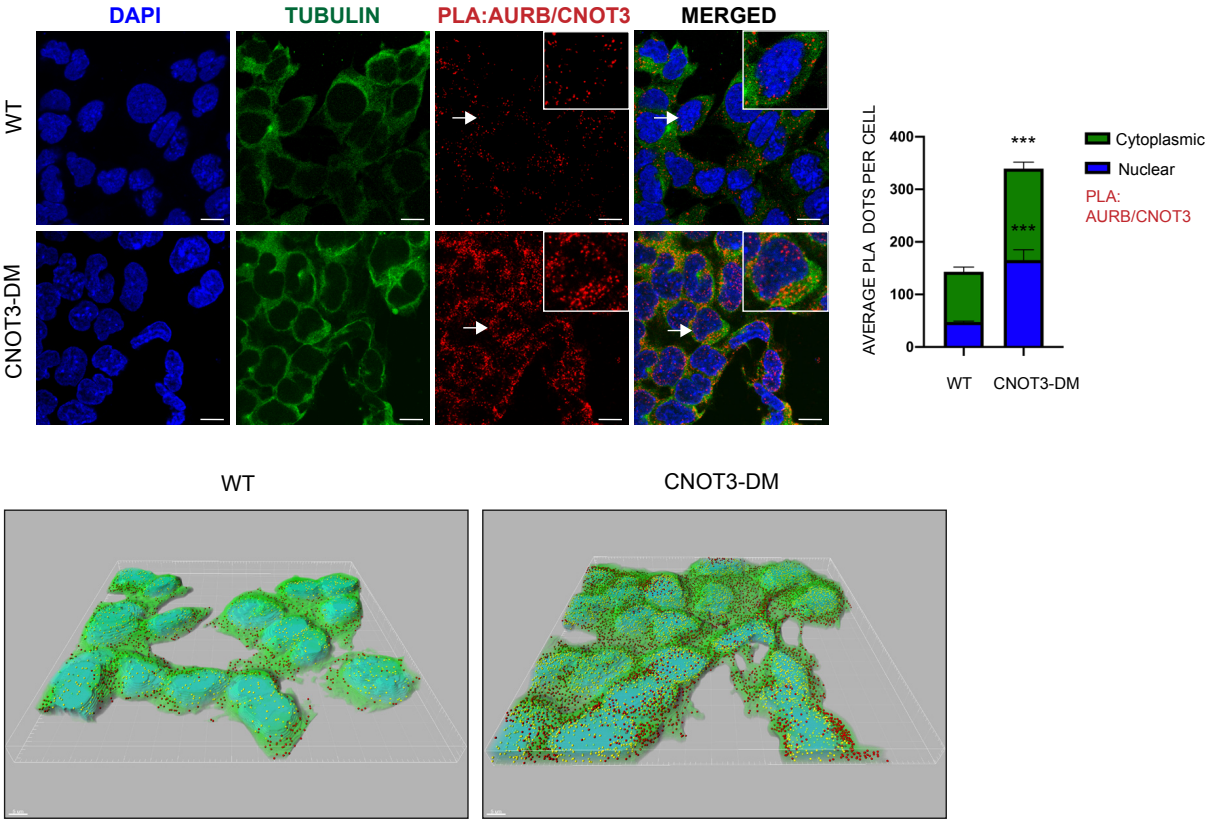

b

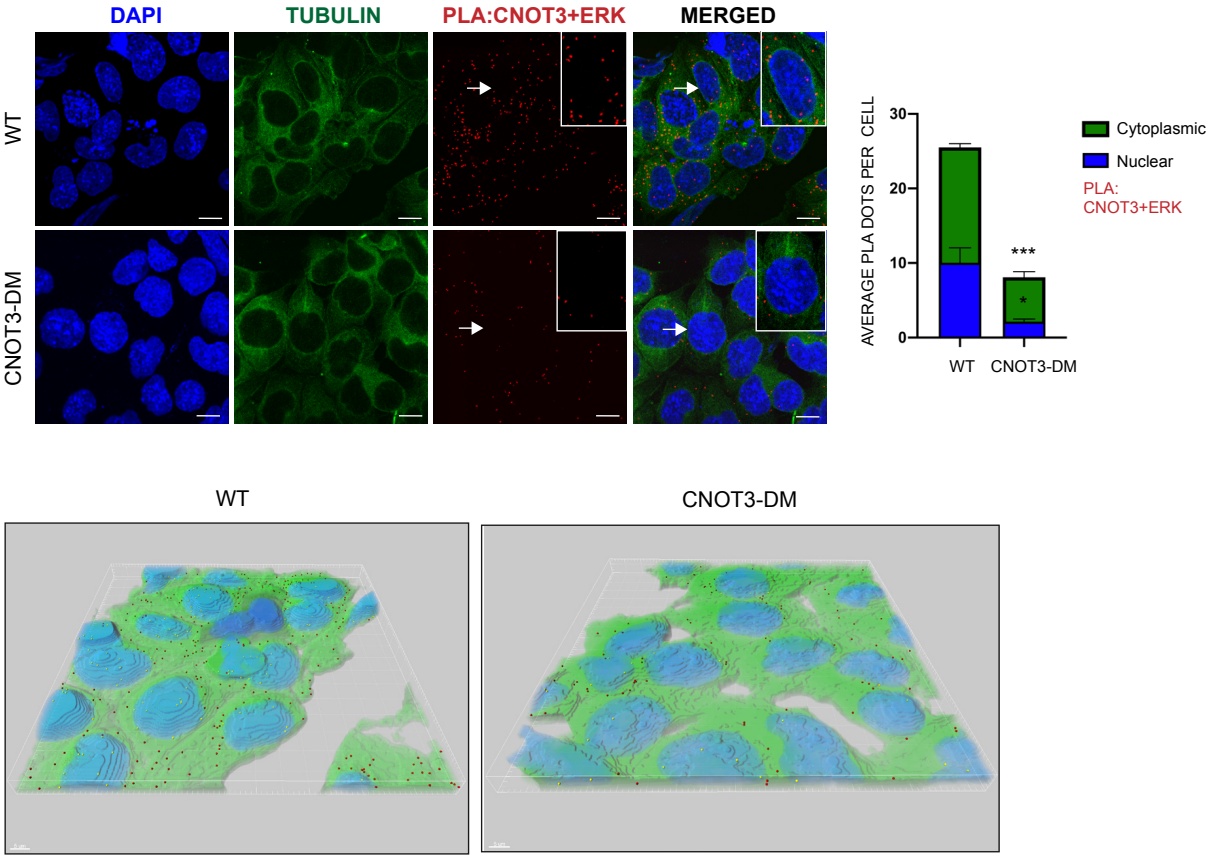

Figure 7: Phosphorylation of CNOT3 alters its interaction with Aurora B and ERK in ME cells. **a**. and **b.** PLA detection of endogenous interaction between Aurora B (AURB) and CNOT3 (**a**) and CNOT3 and ERK (**b**) after 4 days of BMP4 + FGF2 induced differentiation of ME cells from WT and *Cnot3*-DM ESCs. Red dots represent positive PLA signals. Nuclei were stained with DAPI and cytoplasm with anti-tubulin. Boxed areas shown an enlarged image of a cell (indicated by the arrows) from each merged panel (top panel*;* scale bar:10 μm). Three-dimensional images of the cells were digitally reconstructed, showing the distribution of PLA dots in the nucleus (yellow) and cytoplasm (red) (bottom panel; scale bar: 5 μm). (See Methods). PLA dots were quantified from randomly chosen fields from at least 50 cells for each biological replicate. Histograms represent average number of interactions per cell (dots/cell) in the nucleus (blue) and cytoplasm (green). Mean ± SEM; unpaired *t*-test ***P<0.001 (A) *n*=3 (B) *n*=2. Single antibody controls and PLA of CNOT3 and ERK using a second set of antibodies are shown in Supplementary Figure 5.

FIGURE 8

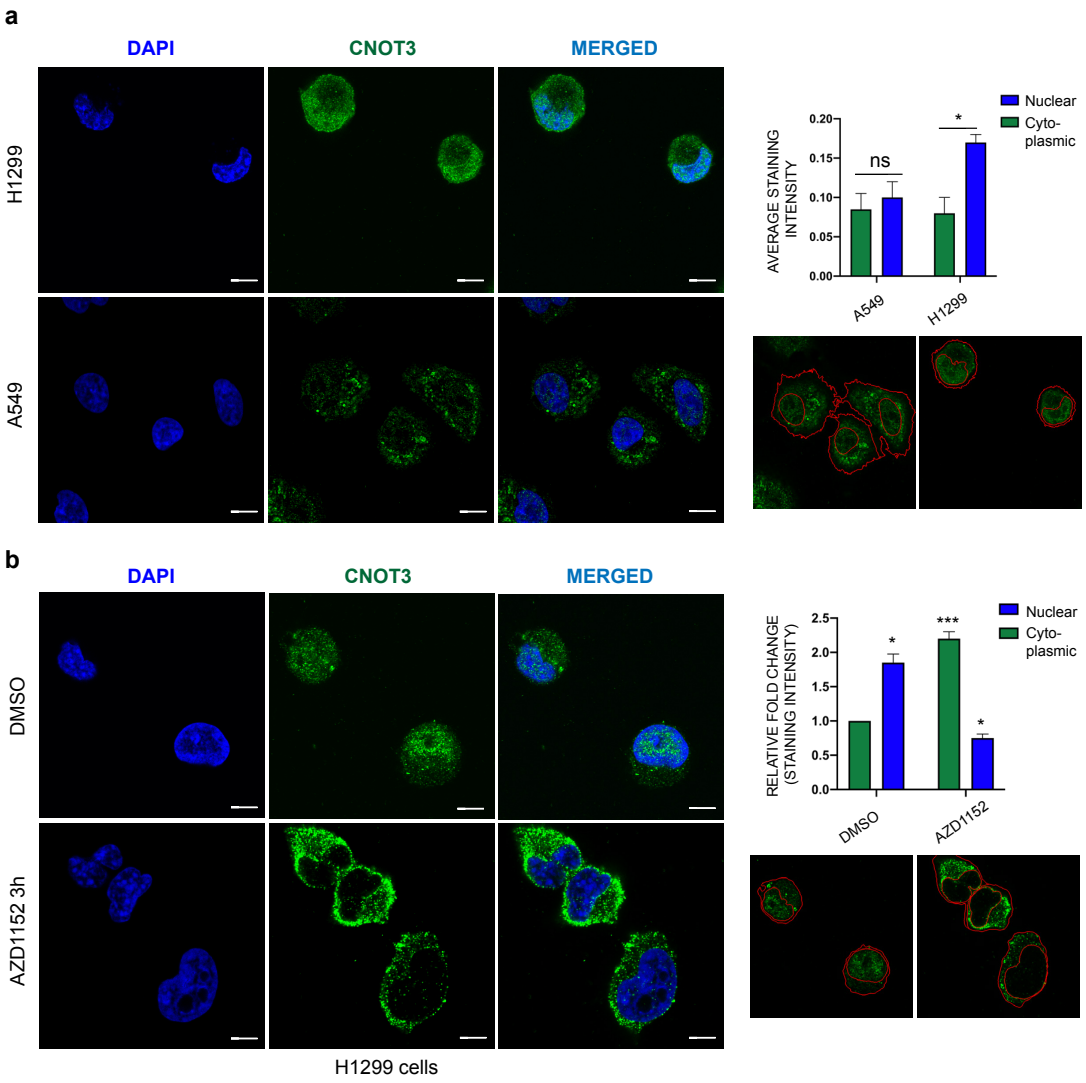

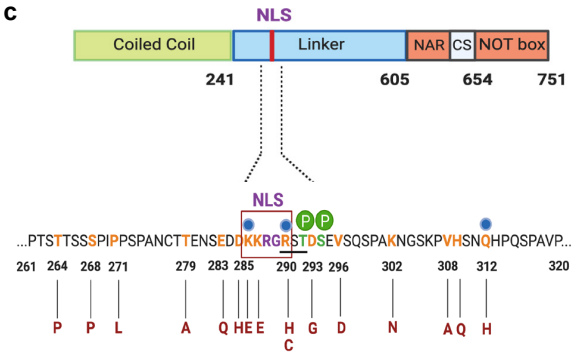

Mutation	Number of patients	Tissue
T264P	1	Thyroid
S268P	1	Upper aerodigestive tract
P271L	1	Lung
T279A	1	Ovary
E283Q	1	Urinary tract
D285H	1	Breast
K286E ●	4	Colon
K287E	1	Colon
R290C ●	2	Colon
R290H ●	2	Lung, Colorectal
D293G	1	Lung
V296D	1	Colon
K302N	1	Endometrium
V308A	1	Liver
H309Q	1	Liver
Q312H ●	2	Liver

NLS

● mutations observed in multiple patients

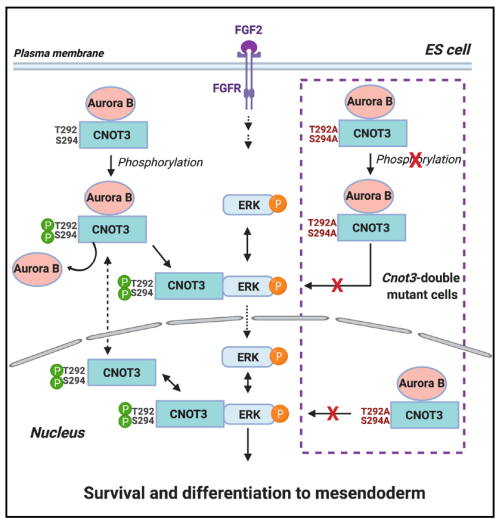

Figure 8: Aurora B phosphorylation promotes nuclear localisation of CNOT3 in a lymph node metastasis NSCLC cell line

a. Comparison of nuclear and cytoplasmic localisation of CNOT3 in two NSCLC cell lines. The H1299 line was derived from a lymph node metastasis and the A549 line from a lung adenoma. Left panel: H1299 cells (top) and A549 cells (bottom) immunostained with anti-CNOT3 and counterstained with DAPI (scale bar: 10 μm). Right panel: Histogram shows digital quantification of the average intensities of the nuclear and cytoplasmic staining for CNOT3 in the H1299 and A549 cells. Mean ± SEM; *n*=3 (unpaired *t*-test *P<0.05). Images (bottom) show representative fields depicting segmentation of the cell and the nuclei used for the quantification. Quantification was performed on at least 30 cells from randomly chosen fields for each biological replicate. **b.** Effect of the Aurora B inhibitor AZD1152 on nuclear and cytoplasmic localization of CNOT3 in H1299 cells. Left panel panel: H1299 cells were incubated for 3 hours with AZD1152 (bottom) or with vehicle (DMSO, top) and were then immunostained as in (**a**) (scale bar = 10 μm). Right panel: Histogram shows quantification of the relative nuclear to cytoplasmic staining for CNOT3 in the AZD1152 and vehicle-treated cells. Fold change was calculated relative to the cytoplasmic staining intensity of the vehicle treated cells. Mean ± SEM; *n*=2 (unpaired *t*-test *P<0.05, ***P<0.001). Images (bottom) show representative fields as in (**a**). Quantification was performed on at least 10 cells from randomly chosen fields for each biological replicate. **c.** Missense mutations described in human cancer patients in the region of the CNOT3 protein spanning residues 261 to 320. Blue spheres indicate mutations that have been observed in more than one patient. The nuclear localisation signal (NLS) is indicated by a red rectangle and the Aurora B

consensus is underlined. **d.** Schematic model showing the proposed role of Aurora B phosphorylation of CNOT3-T292/S294 in promoting the interaction of CNOT3 with phospho-ERK leading to stabilisation of the active form of ERK. The interaction between Aurora B and CNOT3 in wild-type cells is shown on the left. The interaction in the Cnot3-DM cells is illustrated inside the dashed box on the right.

Legend to Supplementary Video 1

Time-lapse imaging of BMP4/FGF2-induced differentiation of wild-type and *Cnot3*-DM ESCs. Images were collected at 30 minute intervals from day 3 to day 7 of the differentiation (see Methods). Scale-bar = 100 μM.

METHODS

Cell Culture

E14 ESCs (female, 129/Ola) were obtained from the LMS Transgenics and ES cell facility. The ESCs were maintained on gelatin coated plates, at 37°C, 5% CO_2, in KnockOut Dulbecco's Modified Eagle's Medium supplemented with 15% fetal bovine serum, 1x NEAA, 2 mM L-glutamine, 100 units/ml penicillin, 100 μg/ml streptomycin, 100 μM βME (all reagents from Thermo Fisher Scientic) and 1000 units/ml LIF (Merck). HEK 293 cells and A549 cells(ATCC) were maintained in Dulbecco's Modified Eagle's Medium supplemented with 10% fetal bovine serum, 2 mM L-glutamine, 100 units/ml penicillin and 100 μg/ml streptomycin. H1299 cells (ATCC) were maintained in RPMI-1640 media supplemented with the same condstituents as mentioned above.

CNOT3 gene editing using CRISPR/Cas9

The guide RNA (gRNA) used to generate the *Cnot3*-T292A/S294A mutant ESCs was 5'-GATTTAGACTTGGACCCACC-3'. The gRNA was cloned into pX330 (Addgene plasmid #42230) using forward primer 5'-CACCGGATTTAGACTTGGACCCACC-3' and reverse primer 5'-AAACGGTGGGTCCAAGTCTAAATCC-3'

The 110 base paired single stranded donor DNA used to target *Cnot3* in exon 10 carrying the mutations was: 5'-ACTCTGAAGATGATAAGAAGAGAGGCCGATCTGCGGATGCTGAAGTCAGCCAGGTGG GTCCAAGTCTAAATCTGATGGTTTGTAACTTGTTTATTGCGTGGTCTCCAAAG-3'

Mouse ESCs ($4x10^6$ cells) were transfected with 3 μg of pX330 plasmid carrying the gRNA, 4 μg of the donor ssDNA and 3 μg of a puromycin resistance plasmid (pCAG-puro^R) using the Mouse ES Cell Nucleofector™ Kit (Lonza) following the manufacturer's protocol. One day post transfection cells were subjected to puromycin selection (1.5 μg/ml) for 24 hours. A week after transfection, individual clones were picked and genotyped by allele specific nested PCR. Mutant genotypes were confirmed by sequencing.

Embryoid bodies

Half a million cells (per well of a six well plate) were seeded on ultra-low attachment plates (Corning Costar) and maintained in KnockOut Dulbecco's Modified Eagle's Medium supplemented with 15% fetal bovine serum, 1x NEAA, 2 mM L-glutamine, 100 units/ml penicillin, 100 μg/ml streptomycin, 100 μM βME and were grown up to 14 days.

Embryoid bodies (EBs) were fixed in 4% paraformaldehyde for twenty minutes followed by permeabilization with 0.5% Triton-X for twenty minutes. Subsequently, EBs were blocked in 3% BSA for one hour and then incubated with primary antibodies overnight at 4°C. On the following day, the EBs were washed 3 times with PBS+0.1 % Tween-20 (PBST) and incubated for 1hour at room temperature with the appropriate secondary antibodies. Embryoid bodies were then washed three times in PBST and incubated with 1μg/ml DAPI in PBS for 45 minutes. Images were acquired using a Leica SP5 confocal microscope (objective x10) with LAS X software (Leica) and images were analysed with Fiji ImageJ software.

Differentiation experiments

ESC differentiation into mesendoderm: Cells were plated at a density of 10000 cells/cm^2 on gelatin-coated plates and incubated in DMEM/F12 KnockOut media containing 64 μg/ml of L Ascorbic acid-2-phosphate magnesium, 543 μg/ml of sodium bicarbonate, 1 μg/ml of heparin, 1x insulin-transferrin-selenium and 2mM Glutamine. For the differentiations, different combinations of signalling factors were added to the medium (see "Treatments of the cells with ligands and inhibitors" below). For time-lapse imaging of differentiation from day 3 to day 7, the plate was transferred to a Zeiss Axiovert 200 microscope with environmental chamber (Solent Scientific Ltd.) and motorised stage (ASI) and images were collected at an interval of thirty minutes. Phase contrast images were acquired in Leica DMIRE2 microscope using the MetaMorph software.

ESC differentiation to endoderm: Cells were plated at a density of 10000 cells/cm^2 on gelatin-coated plates and incubated in high glucose DMEM with

15% FBS, 100 units/ml penicillin, 100 μg/ml streptomycin, 0.1 mM non-essential amino acids, 1mM MTG, 1x GlutaMAX and supplemented with 25 ng/ml of FGF2 (Merck) and 10 μM of retinoic acid (Merck)for 3 days [61].

ESC differentiation to mesoderm: Cells were plated at a density of 15000 cells/cm^2 in gelatin + fibronectin-coated plates and incubated for 4 days in DMEM/F12-Neurobasal (1:1), N2, B27, 1x GlutaMAX, 100 units/ml penicillin, 100 μg/ml streptomycin, 0.1% β-ME and 30 ng/ml of Activin A (R&D Systems).

ESC differentiation to ectoderm: Cells were plated at a density of 15000 cells/cm^2 on gelatin-coated plates and incubated for 4 days in DMEM/F12-Neurobasal medium (1:1), 1x GlutaMAX, 100 units/ml penicillin, 100 μg/ml streptomycin, 100 μM βME, B27 minus Vitamin A and N2.

Treatment of cells with ligands and inhibitors

Aurora B inhibitor AZD1152 (Merck)-200 nM; human recombinant Wnt3 (Cloud-Clone Corp)-200 ng/ml; Activin A (R&D Systems)-100 ng/ml; BMP4 (Merck)-10 ng/ml; FGF2 (Merck)- 25ng/ml; CHIR99021(Merck)-3μM, PD0325901 (Merck)-500nM; U0126(Merck)-10μM; AZD4547 (Abcam)-5nM.

Cell survival assay and Annexin V staining

The Annexin V staining was performed using the FITC Annexin V apoptosis detection kit with PI (BioLegend). The cells were washed with PBS followed by washing with staining buffer and resuspension in binding buffer containing anti-Annexin V and PI and incubation for fifteen minutes at room temperature in the dark. The cells were finally washed with binding buffer and incubated with

1μg/ml DAPI in PBS for 5 minutes. Images were acquired using an Olympus IX70 microscope with Micro-manager software.

Cells were stained with 0.2% crystal violet for a gross estimation of efficiency of differentiation. At different time points of differentiation live and dead cells were distinguished by trypan blue staining and counted manually. Cell survival was measured using Cell Proliferation Reagent WST-1 (Merck) at a final dilution of 1:10 followed by incubation for half an hour and quantitation with a scanning multi-well spectrophotometer (SpectraMax-Molecular Devices).

Immunocytochemistry

All differentiated cells were grown in gelatin coated μ-slides (ibidi) for immunofluorescence. Cells were washed in PBS and fixed in 4% paraformaldehyde for ten minutes followed by permeabilization with 0.5% Triton-X for fifteen minutes. Subsequently, cells were blocked in 3% BSA for one hour and then incubated with primary antibodies overnight at 4°C. After the treatment with primary antibodie,s the cells were washed 3 times with PBST and incubated for 1hour at room temperature with the appropriate secondary antibodies. Subsequently, cells were washed 3 times in PBST and incubated with 1μg/ml DAPI in PBS for 5 minutes. Images were acquired using a Leica SP5 confocal microscope with LAS X software or Olympus IX70 microscope with Micromanager software. Images were analysed with Fiji ImageJ software. CellProfiler software was used for the analysis of images from H1299 and A549 cancer cells.

Expression plasmids

Full length Cnot3 cDNA (OriGene) was cloned in pCDNA 3.2/V5/GW/D-TOPO by PCR addition of restriction sites SmaI/NotI following the manufacturer's instructions. Single Cnot3-T292A, Cnot3-S294A mutant constructs and the T292A/S294A double mutant were generated by site directed mutagenesis and cloned as above. An 8 μg aliquot of each DNA construct was transfected into HEK 293 cells by Calcium Phosphate method.

Immunoprecipitation (IP)

Cells were harvested in IP Lysis Buffer (50 mM Tris-HCl, pH 7.4, 150 mM NaCl, 10% glycerol, 1% Nonidet P-40, 1.0 mM EDTA) with Complete™ protease inhibitor cocktail (Merck). In all cases, 500 μg of total protein was used. The IP procedure was performed using Protein A Sepharose CL-4B beads (GE Healthcare). The extract was pre-cleared with pre-blocked beads (blocked with 1% BSA) for two hours followed by incubation with the desired primary antibodies overnight at 4°C. On the following day, beads were added to it and incubated for another four hours followed by washing the beads twice with wash buffer (50 mM Tris-cl, pH 7.4, 150 mM NaCl, 10% glycerol, 0.5% Nonidet P-40, 1.0 mM EDTA). The immunocomplexes were eluted by boiling with 2x SDS loading buffer.

Protein extractions from cells

To obtain the whole cell extracts, cells were washed with ice cold PBS and the cell pellet was reuspended in Tris lysis buffer (50 mM Tris/HCl pH 7.5, 150 mM

NaCl, 1% Triton X-100, 1 mM DTT, 1 mM Na_3VO_4) with Complete™ protease inhibitor cocktail (Merck).

For preparation of cytoplasmic and nuclear extracts, cells were harvested and re-suspended in harvest buffer containing 10 mM HEPES (pH 7.9), 50 mM NaCl, 0.5 M Sucrose, 0.1 mM EDTA, 0.5% Triton-X 100 and with Complete™ protease inhibitor cocktail (Merck). After obtaining the cytoplasmic extract, the nuclear pellet was further washed with wash buffer/Buffer A (10 mM HEPES (pH 7.9), 10 mM KCL, 0.1 mM EDTA and 0.1 mM EGTA), then re-suspended in Buffer C (10 mM HEPES (pH 7.9), 500 mM NaCl, 0.1 mM EDTA, 0.1 mM EGTA, 0.1% NP40 and protease inhibitor cocktail to extract the nuclear proteins.

Concentrations of the extracts were measured with the Bradford reagent (Bio-Rad).

Immunoblotting

Extracts were diluted in 5x SDS loading buffer, boiled for 5 min and subjected to SDS PAGE. Gels were transferred to nitrocellulose membranes using a Bio-Rad wet tank blotting system. Membranes were blocked with 5% bovine serum albumin (BSA) or 5% milk in TBS+ 0.1% Tween-20 (TBS-T) for 1hour at room temperature and incubated with the primary antibody diluted in 2.5% BSA TBS-T overnight at 4°C. On the following day, membranes were washed 3 times for 20 min with TBS-T, incubated with the appropriate secondary antibody (dilution 1:10000) for 1hour at room temperature, washed again 3 times for 15 minutes and developed using Millipore Crescendo ECL (Merck) using X ray films on Photon Imaging System or Amersham Imager 680.

Protein purification in bacteria

Full length Aurora B cDNA (Dharmacon-Horizon Discovery) and Cnot3$_{275\text{-}480}$ (truncations generated by PCR from full length Cnot3 cDNA) were cloned into pGEX-4T1 and transformed into competent BL21 E.coli cells.

To induce protein expression, β-D-1 thiogalactopyranoside (IPTG) (Merck) was added at a concentration of 0.4 mM and the cells were grown for 3 hours at 37°C. The cell pellets were lysed in lysis buffer (50 mM Tris-Cl pH 8.0, 0.15 M NaCl, 1 mM EDTA) supplemented with Complete™ protease inhibitor cocktail (Merck). Lysozome (100 μg/ml) was added to the mix followed by addition of DTT (1 mM) and 1.5% sarcosyl followed by sonication at intervals of 15 seconds on and 45 seconds off for 5 minutes. The clear supernatants were collected and TritonX-100 was added at a final concentration of 1% and filtered. Glutathione Sepharose High performance (GSH) beads (GE Healthcare), pre-washed in lysis buffer was added followed by overnight incubation at 4°C. Beads were washed with washing buffer (0.5% Triton-X 100 in lysis buffer) and the GST fusion proteins were eluted with elution buffer (10mM glutathione reduced, 5% glycerol in lysis buffer) for 30 minutes at room temperature followed by dialysis in 50 mM Tris-Cl pH 8.0, 0.15 M NaCl, 10% glycerol, 0.5 mM DTT and 0.5mM PMSF.

GST pulldown assay

In order to perform the GST pulldown with GST-Aurora B and Cnot3, pCDNA-*Cnot3* was *in vitro* transcribed/translated using a TNT® Quick Coupled Transcription/Translation kit (Promega) according to manufacturer's instructions. An aliquot (0.5 μg) of the plasmid was incubated with 20 μl of TNT

T7 quick Master Mix, 1 µl of ^{35}SMethionine 10µCi and water to a final volume of 25 µl. The transcription/translation reaction was performed for 90 minutes at 30°C.

1µg of GST or GST-Aurora B was added to GSH beads in binding buffer (50 mM Tris-cl pH 8.0, 150 mM monopotassium glutamate, 1mM EDTA, 0.1 % Igepal CAL630, 5% glycerol, 0.2% BSA) and supplemented with Complete™ protease inhibitor cocktail (Merck), and incubated for two hours at 4°C. The beads were then washed and 5 µl of the *in vitro* transcribed/translated Cnot3 was incubated with the beads overnight at 4°C. The beads were then washed with the binding buffer and the proteins were eluted by boiling in loading buffer. The eluted proteins were subjected to SDS-PAGE, stained, dried for one hour at 80°C and exposed to Xray film.

In vitro kinase assay

Purified GST-CNOT3 fragments (1 µg) were incubated with 80 ng of His-Aurora B (MRC PPU, College of Life Sciences, University of Dundee, Scotland, mrcppureagents.dundee.ac.uk) for 30 min at 30°C in phosphorylation buffer (50 mM TrisHCl pH 7.5, 10 mM $MgCl_2$, 500 µM ATP, 1 mM DTT, 5 mM NaF, 1 µl of ^{32}Pγ-ATP 10µCi). Reactions were stopped by addition of SDS loading buffer, boiled for 5 min and subsequently run on SDS PAGE. The gel was dried and exposed to X ray film at -80°C.

Flow cytometry

Cells were trypsinised, washed twice with PBS, fixed with 70% ethanol for 30 min on ice and washed twice with 2% FCS-PBS. Subsequently, cells were resuspended in PBS containing 1μg/ml RNAse A (Thermo Fisher Scientific), 50 μg/ml propidium iodide and 0.05% NP40, incubated 20 min at room temperature in the dark followed by analysis. Anaysis was performed on an LSRII Flow Cytometer (Becton-Dickinson) and data was analysed using FlowJo Software.

RNA sequencing

Total RNA was extracted from $2x10^6$ cells (3 biological replicates for wild-type and CNOT3-DM cells) using Trizol reagent (Thermo Fisher Scientific) following the manufacturer's instructions. A 2 μl aliquot of a 1:10 dilution of the ERCC RNA Spike-in Mix (Thermo Fisher Scientific) were added to each sample. The quality of the extracted RNA was analysed using the RNA 6000 Nano kit on a 2100 Bioanalyzer (Agilent). An aliquot of 500 ng of RNA was used to prepare a polyadenylated RNA library with the TruSeq Stranded mRNA Library Prep Kit (Illumina) following the manufacturer's protocol. RNA libraries were sequenced in one lane by multiplexing on an Illumina HiSeq 2500 sequencer with a 100 bp read output.

RNAseq reads were aligned against to Ensembl Mouse genome (NCBIM37) reference sequence assembly and transcript annotation that obtained from Illumina iGenomes (https://support.illumina.com/sequencing/sequencing_software/igenome.html, and to ERCC reference with Tophat2 (2.0.11) [62, 63]. Gene-based read counts and

ERCC counts were obtained using featureCounts function from Rsubread Bioconductor package [63, 64]. Differentially expressed gene analysis was performed with DESeq2 Bioconductor package [65] after normalising the data against ERCC with RUVseq Bioconductor package [66]. Differentially expressed genes were defined with Benjamini-Hochberg adjusted p-value<0.05 and fold change ratio > 1.5. Gene ontology analysis was performed with goseq Bioconductor package [67]. After converting mouse gene symbol to human gene symbol using the report of Human and Mouse Homology retrieved from Mouse Genome Informatics (MGI, http://www.informatics.jax.org), Gene Set Enrichment Analysis (GSEA) [68, 69] was then performed with GseaPreranked tool using Hallmarks gene set (h.all.v5.2.symbols.gmt).

Proximity ligation assay (PLA)

PLA was performed using the Duolink In Situ Red Starter Kit Mouse/Rabbit (Merck) following manufacturer's instructions. Cells were fixed and permeabilised following standard conditions as described above followed by incubation with blocking buffer (provided in the kit) for one hour at 37°C. Subsequently, cells were incubated with desired antibodies and single antibody controls overnight at 4°C. After the primary antibodies, the cells were washed with wash buffers and incubated with mouse and rabbit probes for one hour at 37°C followed by ligation reaction at 37°C for half an hour. The amplification reaction of the ligated product was then carried out at 37°C for 90 minutes followed by counterstaining with FITC-αTubulin for forty minutes at room temperature. The cells were finally washed and incubated with 1μg/ml DAPI in PBS for 5 minutes. Images were acquired using a Leica SP5 confocal microscope

with LAS X software. PLA dots were analysed and quantified using Imaris - Bitplane software (Oxford Instruments). Three-dimensional segmentation and digital image reconstructions of the cells were carried out using Imaris Spots and Surfaces packages.

Mass spectrometry

Peptides were separated using an Ultimate 3000 RSLC nano liquid chromatography system (Thermo Fisher Scientific) coupled to an LTQ Velos Orbitrap mass spectrometer (Thermo Fisher Scientific) via a Dionex nano-esi source. Eluted peptides were analysed by the LTQ Velos operating in positive polarity using a data-dependent acquisition mode. Ions for fragmentation were determined from an initial MS1 survey scan at 60000 resolution (at m/z 200). Ion Trap CID (collisional induced dissociation), Ion Trap CID-MSA (MultiStage Activation) and HCD (Higher energy collisional induced dissociation) were carried out concurrently on the top 3 most abundant ions. For CID fragmentation methods MS1 and MS2 MSn AGC targets set to 1e6 and 1e4 for 1 microscan and a maximum injection time of 500ms and 100ms respectively. A survey scan m/z range of 350 – 1500 was used, with a normalised collision energy set to 35% for both CID and HCD, charge state rejection enabled for +1 ions and a minimum threshold for triggering fragmentation of 500 counts.

RNA isolation and quantitative RT-PCR (qPCR)

Total RNA was isolated with TRIzol reagent (Thermo Fisher Scientific) following manufacturer's instructions. cDNA was synthesized with RevertAid First Strand cDNA Synthesis Kit (Thermo Fisher Scientific) using 200 ng of RNA following the

manufacturer's protocol. qPCRs were performed using Sensimix SYBR NORox SYBR GREEN (Bioline). Each PCR was performed in duplicate using 1 μl of cDNA (from 20 μl reaction) and 200 nM primer concentration.

Gene expression was determined relative to *MLN 51* transcript levels. The primers used in this analysis are listed in Supplementary Table 1.

Statistical analysis

All statistical analyses were performed with GraphPad Prism software. The statistical tests used in each experiment and significances are indicated in the corresponding figure legends.

Data availability

The RNA-seq data is in the process of being deposited in the NCBI GEO database.

REFERENCES

1. Stern, C.D. & Downs, K.M. The hypoblast (visceral endoderm): an evo-devo perspective. *Development* **139**, 1059-1069 (2012).
2. Wang, L. & Chen, Y.G. Signaling Control of Differentiation of Embryonic Stem Cells toward Mesendoderm. *Journal of molecular biology* **428**, 1409-1422 (2016).
3. Tsakiridis, A. *et al.* Distinct Wnt-driven primitive streak-like populations reflect in vivo lineage precursors. *Development* **141**, 1209-1221 (2014).
4. Ben-Haim, N. *et al.* The nodal precursor acting via activin receptors induces mesoderm by maintaining a source of its convertases and BMP4. *Developmental cell* **11**, 313-323 (2006).
5. Fujiwara, T., Dehart, D.B., Sulik, K.K. & Hogan, B.L. Distinct requirements for extra-embryonic and embryonic bone morphogenetic protein 4 in the formation of the node and primitive streak and coordination of left-right asymmetry in the mouse. *Development* **129**, 4685-4696 (2002).
6. Bernardo, A.S. *et al.* BRACHYURY and CDX2 mediate BMP-induced differentiation of human and mouse pluripotent stem cells into embryonic and extraembryonic lineages. *Cell stem cell* **9**, 144-155 (2011).

7. Tremblay, K.D., Hoodless, P.A., Bikoff, E.K. & Robertson, E.J. Formation of the definitive endoderm in mouse is a Smad2-dependent process. *Development* **127**, 3079-3090 (2000).
8. Sui, L., Bouwens, L. & Mfopou, J.K. Signaling pathways during maintenance and definitive endoderm differentiation of embryonic stem cells. *Int J Dev Biol* **57**, 1-12 (2013).
9. Yu, P., Pan, G., Yu, J. & Thomson, J.A. FGF2 sustains NANOG and switches the outcome of BMP4-induced human embryonic stem cell differentiation. *Cell stem cell* **8**, 326-334 (2011).
10. Roux, P.P. & Blenis, J. ERK and p38 MAPK-activated protein kinases: a family of protein kinases with diverse biological functions. *Microbiol Mol Biol Rev* **68**, 320-344 (2004).
11. Kolch, W. Coordinating ERK/MAPK signalling through scaffolds and inhibitors. *Nat Rev Mol Cell Biol* **6**, 827-837 (2005).
12. Sacks, D.B. The role of scaffold proteins in MEK/ERK signalling. *Biochemical Society transactions* **34**, 833-836 (2006).
13. Collart, M.A. The Ccr4-Not complex is a key regulator of eukaryotic gene expression. *Wiley Interdiscip Rev RNA* **7**, 438-454 (2016).
14. Hu, G. *et al.* A genome-wide RNAi screen identifies a new transcriptional module required for self-renewal. *Genes Dev* **23**, 837-848 (2009).
15. Zheng, X. *et al.* Cnot1, Cnot2, and Cnot3 maintain mouse and human ESC identity and inhibit extraembryonic differentiation. *Stem cells (Dayton, Ohio)* **30**, 910-922 (2012).
16. Neely, G.G. *et al.* A global in vivo Drosophila RNAi screen identifies NOT3 as a conserved regulator of heart function. *Cell* **141**, 142-153 (2010).
17. Yang, C.Y. *et al.* Interaction of CCR4-NOT with EBF1 regulates gene-specific transcription and mRNA stability in B lymphopoiesis. *Genes Dev* **30**, 2310-2324 (2016).
18. Li, X. *et al.* Adipocyte-specific disruption of mouse Cnot3 causes lipodystrophy. *FEBS Lett* **591**, 358-368 (2017).
19. De Keersmaecker, K. *et al.* Exome sequencing identifies mutation in CNOT3 and ribosomal genes RPL5 and RPL10 in T-cell acute lymphoblastic leukemia. *Nat Genet* **45**, 186-190 (2013).
20. Shirai, Y.T. *et al.* CNOT3 targets negative cell cycle regulators in non-small cell lung cancer development. *Oncogene* **38**, 2580-2594 (2019).
21. Cejas, P. *et al.* Transcriptional Regulator CNOT3 Defines an Aggressive Colorectal Cancer Subtype. *Cancer Res* **77**, 766-779 (2017).
22. Forbes, S.A. *et al.* COSMIC: somatic cancer genetics at high-resolution. *Nucleic Acids Res* **45**, D777-D783 (2017).
23. Priestley, P. *et al.* Pan-cancer whole-genome analyses of metastatic solid tumours. *Nature* (2019).
24. Carmena, M., Wheelock, M., Funabiki, H. & Earnshaw, W.C. The chromosomal passenger complex (CPC): from easy rider to the godfather of mitosis. *Nat Rev Mol Cell Biol* **13**, 789-803 (2012).
25. Song, J., Salek-Ardakani, S., So, T. & Croft, M. The kinases aurora B and mTOR regulate the G1-S cell cycle progression of T lymphocytes. *Nat Immunol* **8**, 64-73 (2007).

26. Trakala, M., Fernandez-Miranda, G., Perez de Castro, I., Heeschen, C. & Malumbres, M. Aurora B prevents delayed DNA replication and premature mitotic exit by repressing p21(Cip1). *Cell Cycle* **12**, 1030-1041 (2013).
27. Takeshita, M. *et al.* Aurora-B overexpression is correlated with aneuploidy and poor prognosis in non-small cell lung cancer. *Lung Cancer* **80**, 85-90 (2013).
28. Tuncel, H. *et al.* Nuclear Aurora B and cytoplasmic Survivin expression is involved in lymph node metastasis of colorectal cancer. *Oncology letters* **3**, 1109-1114 (2012).
29. Zhang, Y. *et al.* Elevated Aurora B expression contributes to chemoresistance and poor prognosis in breast cancer. *Int J Clin Exp Pathol* **8**, 751-757 (2015).
30. Frangini, A., Vol. PhD (Imperial College London, 2013).
31. Donchet, A. *et al.* The structure of the nucleoprotein of Influenza D shows that all Orthomyxoviridae nucleoproteins have a similar NPCORE, with or without a NPTAIL for nuclear transport. *Scientific reports* **9**, 600 (2019).
32. Dixon, S.E., Bhatti, M.M., Uversky, V.N., Dunker, A.K. & Sullivan, W.J., Jr. Regions of intrinsic disorder help identify a novel nuclear localization signal in Toxoplasma gondii histone acetyltransferase TgGCN5-B. *Mol Biochem Parasitol* **175**, 192-195 (2011).
33. Tang, Y.S., Lo, C.Y., Mok, C.K., Chan, P.K. & Shaw, P.C. The Extended C-Terminal Region of Influenza C Virus Nucleoprotein Is Important for Nuclear Import and Ribonucleoprotein Activity. *J Virol* **93** (2019).
34. Chuai, M., Hughes, D. & Weijer, C.J. Collective epithelial and mesenchymal cell migration during gastrulation. *Curr Genomics* **13**, 267-277 (2012).
35. Wolfe, A.D. & Downs, K.M. Mixl1 localizes to putative axial stem cell reservoirs and their posterior descendants in the mouse embryo. *Gene Expr Patterns* **15**, 8-20 (2014).
36. Costello, I. *et al.* Lhx1 functions together with Otx2, Foxa2, and Ldb1 to govern anterior mesendoderm, node, and midline development. *Genes Dev* **29**, 2108-2122 (2015).
37. Bertocchini, F. & Stern, C.D. The hypoblast of the chick embryo positions the primitive streak by antagonizing nodal signaling. *Developmental cell* **3**, 735-744 (2002).
38. Vallier, L. *et al.* Early cell fate decisions of human embryonic stem cells and mouse epiblast stem cells are controlled by the same signalling pathways. *PLoS One* **4**, e6082 (2009).
39. Bakre, M.M. *et al.* Generation of multipotential mesendodermal progenitors from mouse embryonic stem cells via sustained Wnt pathway activation. *J Biol Chem* **282**, 31703-31712 (2007).
40. Alexanian, M. *et al.* A transcribed enhancer dictates mesendoderm specification in pluripotency. *Nature Communications* **8**, 1806 (2017).
41. Yamaguchi, T.P., Harpal, K., Henkemeyer, M. & Rossant, J. fgfr-1 is required for embryonic growth and mesodermal patterning during mouse gastrulation. *Genes Dev* **8**, 3032-3044 (1994).
42. Deng, C.X. *et al.* Murine FGFR-1 is required for early postimplantation growth and axial organization. *Genes Dev* **8**, 3045-3057 (1994).

43. Ciruna, B. & Rossant, J. FGF signaling regulates mesoderm cell fate specification and morphogenetic movement at the primitive streak. *Developmental cell* **1**, 37-49 (2001).
44. Xu, X. *et al.* Fibroblast growth factor receptor 2 (FGFR2)-mediated reciprocal regulation loop between FGF8 and FGF10 is essential for limb induction. *Development* **125**, 753-765 (1998).
45. Kunath, T. *et al.* FGF stimulation of the Erk1/2 signalling cascade triggers transition of pluripotent embryonic stem cells from self-renewal to lineage commitment. *Development* **134**, 2895-2902 (2007).
46. Lanner, F. & Rossant, J. The role of FGF/Erk signaling in pluripotent cells. *Development* **137**, 3351-3360 (2010).
47. Wang, Q., Zhou, Y., Wang, X. & Evers, B.M. Glycogen synthase kinase-3 is a negative regulator of extracellular signal-regulated kinase. *Oncogene* **25**, 43-50 (2006).
48. Jeong, W.-J., Ro, E.J. & Choi, K.-Y. Interaction between Wnt/β-catenin and RAS-ERK pathways and an anti-cancer strategy via degradations of β-catenin and RAS by targeting the Wnt/β-catenin pathway. *npj Precision Oncology* **2**, 5 (2018).
49. Bonet, C. *et al.* Aurora B is regulated by the mitogen-activated protein kinase/extracellular signal-regulated kinase (MAPK/ERK) signaling pathway and is a valuable potential target in melanoma cells. *J Biol Chem* **287**, 29887-29898 (2012).
50. Mebratu, Y. & Tesfaigzi, Y. How ERK1/2 activation controls cell proliferation and cell death: Is subcellular localization the answer? *Cell Cycle* **8**, 1168-1175 (2009).
51. Sasai, K., Katayama, H., Hawke, D.H. & Sen, S. Aurora-C Interactions with Survivin and INCENP Reveal Shared and Distinct Features Compared with Aurora-B Chromosome Passenger Protein Complex. *PLoS One* **11**, e0157305 (2016).
52. Delacruz, R.G.C. *et al.* Functional characterization of CNOT3 variants identified in familial adenomatous polyposis adenomas. *Oncotarget* **10**, 3939-3951 (2019).
53. Giannakis, M. *et al.* Genomic Correlates of Immune-Cell Infiltrates in Colorectal Carcinoma. *Cell reports* **15**, 857-865 (2016).
54. Deschenes-Simard, X. *et al.* Tumor suppressor activity of the ERK/MAPK pathway by promoting selective protein degradation. *Genes Dev* **27**, 900-915 (2013).
55. Hamilton, W.B. & Brickman, J.M. Erk signaling suppresses embryonic stem cell self-renewal to specify endoderm. *Cell reports* **9**, 2056-2070 (2014).
56. Carballada, R., Yasuo, H. & Lemaire, P. Phosphatidylinositol-3 kinase acts in parallel to the ERK MAP kinase in the FGF pathway during Xenopus mesoderm induction. *Development* **128**, 35-44 (2001).
57. Ma, X., Chen, H. & Chen, L. A dual role of Erk signaling in embryonic stem cells. *Exp Hematol* **44**, 151-156 (2016).
58. Caunt, Christopher J. & McArdle, Craig A. ERK phosphorylation and nuclear accumulation: insights from single-cell imaging. *Biochemical Society transactions* **40**, 224-229 (2012).

59. Pouysségur, J. & Lenormand, P. Fidelity and spatio-temporal control in MAP kinase (ERKs) signalling. *European Journal of Biochemistry* **270**, 3291-3299 (2003).
60. Boland, A. *et al.* Structure and assembly of the NOT module of the human CCR4-NOT complex. *Nature structural & molecular biology* **20**, 1289-1297 (2013).
61. Kim, J.S., Kim, B.S., Kim, J., Park, C.S. & Chung, I.Y. The phosphoinositide-3-kinase/Akt pathway mediates the transient increase in Nanog expression during differentiation of F9 cells. *Arch Pharm Res* **33**, 1117-1125 (2010).
62. Kim, D. *et al.* TopHat2: accurate alignment of transcriptomes in the presence of insertions, deletions and gene fusions. *Genome biology* **14**, R36 (2013).
63. Liao, Y., Smyth, G.K. & Shi, W. featureCounts: an efficient general purpose program for assigning sequence reads to genomic features. *Bioinformatics (Oxford, England)* **30**, 923-930 (2014).
64. Liao, Y., Smyth, G.K. & Shi, W. The Subread aligner: fast, accurate and scalable read mapping by seed-and-vote. *Nucleic Acids Res* **41**, e108 (2013).
65. Love, M.I., Huber, W. & Anders, S. Moderated estimation of fold change and dispersion for RNA-seq data with DESeq2. *Genome biology* **15**, 550 (2014).
66. Risso, D., Ngai, J., Speed, T.P. & Dudoit, S. Normalization of RNA-seq data using factor analysis of control genes or samples. *Nature biotechnology* **32**, 896-902 (2014).
67. Young, M.D., Wakefield, M.J., Smyth, G.K. & Oshlack, A. Gene ontology analysis for RNA-seq: accounting for selection bias. *Genome biology* **11**, R14 (2010).
68. Subramanian, A. *et al.* Gene set enrichment analysis: a knowledge-based approach for interpreting genome-wide expression profiles. *Proc Natl Acad Sci U S A* **102**, 15545-15550 (2005).
69. Mootha, V.K. *et al.* PGC-1alpha-responsive genes involved in oxidative phosphorylation are coordinately downregulated in human diabetes. *Nat Genet* **34**, 267-273 (2003).